Supplemental Information

Differential stoichiometry among core ribosomal proteins

Nikolai Slavov, Stefan Semrau, Edoardo Airoldi, Bogdan A. Budnik, Alexander van Oudenaarden

Correspondence should be addressed to: nslavov@alum.mit.edu

This PDF file includes:

Supplemental Experimental Procedures

Supplemental Discussion

Supplemental Figures S1 to S5

Supplemental References

Captions for Supplemental Tables S1 to S5

Supplemental Experimental Procedures

Cultivation of mouse ESC

Mouse embryonic stem cells (E14 10^{th} passage) were grown as adherent cultures in 10 cm plates with 10 ml DMEM/F12 media supplemented with 10 % knockout serum replacement, nonessential amino acids (NEAA supplement), 0.1 mM β-mercapto-ethanol, 1 % penicillin and streptomycin, leukemia inhibitory factor (LIF; 1,000 U LIF/ml), and $2i$ (GSK3β and Mek 1/2 inhibitors). The growth curve in Figure S1A indicates that the cells grew exponentially at a growth rate of 0.08 per hour, which corresponds to 9 hours doubling time. During the middle of the exponential growth period, the cells were detached from the plate by 2 min incubation with accutase (Millipore) at 37 ^oC. The cells were pelleted by a 2 min centrifugation, and the pellet was frozen immediately in liquid nitrogen.

Cultivation of yeast

All yeast experiments used a prototrophic diploid strain (DBY12007) with a S288c background and wild type HAP1 alleles (Hickman and Winston, 2007). We grew our cultures in a commercial bioreactor (LAMBDA Laboratory Instruments) using minimal media with the composition of yeast nitrogen base (YNB) and supplemented with 2 g/L D-glucose. Before inoculation, the reactor was filled with 2 L of minimal media and warmed up to a working temperature of 30^oC. Then cultures were started by inoculating the media with 100 μl overnight culture from DBY12007. The overnight cultures were prepared by first streaking frozen DBY12007 on YPD plates (YPD; 10 g of Bacto-Yeast extract, 20 g of Bacto-peptone, 20 g of Bacto-agar, and 20 g of glucose in 1000 ml of water) and then growing a single colony in the same minimal media used for the subsequent growth experiment in the bioreactor. The density of the culture used for inoculation was 2×10^7 cells per ml, resulting in an initial density of 10^3 cells/ml for the culture in the reactor. The cultures were grown at 30^oC and continuously stirred to ensure their homogeneity. The culture was aerated with air coming from a compressed gas cylinder (Airgas, AI-B300 breathable air). The incoming flow of air was controlled by a thermal-based mass-flow controller and filtered through a 0.2 μm filter to ensure sterility.

Cell density was measured on Beckman-Coulter Multisizer 4 by counting at least 20,000 single cells (Slavov *et al*, 2011; Slavov and Botstein, 2011). The samples were taken during the first exponential growth phase on glucose carbon source and during the second exponential growth phase on ethanol carbon source (Slavov *et al*, 2014). To take samples without disturbing the cultures, we used a metal tube attached to silicon tubing and a syringe. The metal tube could be inserted in and out of the cultures, and the syringe used to sample the required volume quickly from the homogeneous cultures. The sampling tubing was kept sterile and no culture was left in it after sampling. All samples were immediately filtered, frozen in liquid nitrogen, and processed as described below.

Sucrose gradients and mass spectrometry work flow

Both yeast and mouse embryonic stem cells were lysed by vortexing for 10 min with glass beads in cold PLB (20 mM HEPES-KOH at pH 7.4, 1 % Triton X–100, 2 mM Magnesium Acetate, 100 mM Potassium Acetate, 0.1 mg/ml cycloheximide, and 3 mM DTT). The crude

extracts obtained from this lysis procedure were clarified by centrifugation, and the resulting supernatants were applied to linear 11 ml sucrose gradients ($10\ \% - 50\ \%$) and spun at 35,000 rpm in a Beckman SW41 rotor either for 3 hours (for yeast samples) or for 2.5 hours (for mouse samples). Twelve fractions from each sample were collected using a Gradient Station (BioComp, Cat. # 153-001). The RNA profile across the gradient was measured by Gradient Profiler (BioComp).

Sample preparation

If ribosomes from different sucrose fractions have different stability and/or susceptibility to digestion, incomplete break-down and digestion of ribosomes may influence our quantification. While such differential stability is interesting on its own right, we wanted to clearly separate it from differential protein content, i.e., RP stoichiometry. To achieve that, we used multiple very harsh sample-preparation protocols that powerfully break-down and denature proteins and their complexes. These protocols include: (i) concentrated guanidinium chloride, (ii) 2 % SDS, (iii) SDS gel, and (iv) chloroform acetone precipitation. Samples prepared with these harsh methods resulted in very similar estimates of RP stoichiometry, suggesting that the harsh protocols succeeded in breaking down completely the ribosomes from all fractions. Furthermore, the relative RP levels estimated from MS and western blots are very similar (Figure S3), providing additional evidence that differential stability of ribosomes and/or partial RP digestion are not major factors affecting our data.

The RP levels displayed in the main figures were estimated from sucrose samples broken down by guanidinium chloride: To break-down the ribosomes completely, the analyzed volume from each sucrose fraction was mixed with 4 volumes of 8 M guanidinium chloride and vortexed for at least 10 min at 37 ^oC. This approach is simple to perform and has the advantage of avoiding potential artifacts associated with protein precipitation. For each fraction, the rRNA absorbance measured during sucrose gradient fractions (Figure 1A, Figure 3A, B) corresponded well with the summed precursor-ion-areas of RP peptides, further supporting that ribosomes are broken-down and and their proteins quantified with uniform efficiency across sucrose fractions. The denatured proteins from each sucrose fraction were further processed via the FASP protocol (Wiśniewski *et al*, 2009), and digested with either lys-C or a mixture of trypsin and lys-C (Promega; # V5073). The digestion with the trypsin/lys-C mix resulted in more identified and

quantified peptides, Figure S2. Subsequently each sample was labeled with TMT reagent (Prod # 90061, Thermo Fisher, San Jose, CA) according to the manufacturer's protocol.

Tandem Mass Tags (TMT) mass spectrometry

The labeled set–sample was injected from an auto–sampler into the trapping column (75 μm column ID, 5 cm packed with 5 μm beads on 20 nm pores, from Michrom Bioresources, Inc.) and washed for 15 min; the sample was eluted to analytic column with a gradient from 2 to 32 % of buffer B (0.1 % formic acid in ACN) over 180 min gradient and fed into LTQ Orbitrap Elite (Thermo Fisher, San Jose, CA). The instrument was set to run in TOP 20 MS/MS mode method with dynamic exclusion. After MS1 scan in Orbitrap with 60K resolving power, each ion was submitted to an HCD MS/MS with 15K or 30K resolving power and to CID MS/MS scan subsequently. All quantification data were derived from HCD spectra.

Analysis of mass spectrometry spectra

Mass/charge spectra where analyzed by MaxQuant (Cox and Mann, 2008) (version 1.4.1.2), SEQUEST HT (Eng *et al*, 1994) and Mascot (Cottrell and London, 1999) (Version 2.4.1) run via the Proteome Discover (64bit version 1.4.0.288, Thermo), and standalone Mascot. All searches were run on a Windows server 2008 64 bit operating system with 64 CPU blades and 256 GB of RAM with the following general parameters. Parent ion mass tolerance was set to 20 ppm, mass tolerance for MS/MS ions was set to 0.02 Da for HCD and to 0.6 Da for CID spectra. For all searches, minimal peptide length was specified as 6 amino acids and maximal peptide length as 50 amino acids. The peptide charge state was limited to +7 for searches with MaxQuant. Searches were performed against either the yeast or the mouse uniprot database and common contaminants that were added to the database. Searches had trypsin or lys-C enzyme specificity, allowing 2 missed cleavages. Asn and Gln deamidation and Met oxidation were included as variable modifications in the search parameters.

The search results from all search engines were filtered at 1 % false discovery rate (FDR) on both protein and on peptide levels using the Percolator (Version 2.05 Build Date May 6 2013). The results exported for further analysis included all peptide spectrum matches (PSM) that were assigned to one or more proteins and passed the statistical significance filter. These results

were outputted in the "Evidence File" for MaxQuant and in a peptide–level–results text file for Proteome Discover. The Proteome Discover files are provided as supplementary datasets.

Similar to Schwanhäusser *et al* (2011), we estimated the absolute abundance of proteins by their iBAQ score, since these scores are among the simplest metrics that allow state-of-the-art accuracy of absolute protein quantification. However, the accuracy of all methods for absolute protein quantification, including the iBAQ score, is undermined by extraneous factors, including protein digestion efficiency, peptide ionization efficiency, the presence of co-eluting peptides, and chromatographic aberrations (Peng *et al*, 2012; Lu *et al*, 2006). These extraneous factors can be averaged out in relative protein quantification, i.e., quantifying the same peptide/protein quantified across different fractions or relative to a standard, allowing errors below $10\ \%$ (Ong *et al*, 2002; Blagoev *et al*, 2004; Bantscheff *et al*, 2007; Chen and Williamson, 2013; Altelaar *et al*, 2013). Throughout all main figures, we use this type of relative quantification that is derived from the reporter-ion-intensities (MS2-level); the relative level of each RP is estimated as the median of the relative reporter-ion-intensities of its unique peptides; This relative quantification makes possible much higher accuracy than iBAQ scores do, but does not allow to directly compare the abundances of different proteins. Thus we have chosen to limit our analysis of differential RP stoichiometries to relative-quantification, which is the most quantitatively accurate and unbiased data that current MS methods can provide.

Western blots

The variable RP stoichiometry indicated by our MS data is rather surprising given that for decades the ribosome has been considered the preeminent example of a large RNA–protein complex with a fixed stoichiometry among the constituent core RPs. Thus, we sought to use an independent experimental method, Western blots, to test out findings. While Western blots have lower sensitivity, specificity, and accuracy than MS (Aebersold *et al*, 2013), they also quantify proteins based on an orthogonal method to MS and are thus an excellent method for further testing the variability of the RP stoichiometry.

Because of the lower sensitivity of Western blots, the low–passage E14 ESCs used for the MS measurements did not provide enough protein material for reliable quantification of the polysomes by Western blots. Thus, we used higher passage–number E14 strain that grows

faster and provides enough protein for reliable quantification. We estimated that $5\ \mu l$ of the monosomal fraction and $20\ \mu l$ of the polysomal fraction having $7-10$ ribosomes per mRNAs have about equal amounts of total ribosomal protein, and we validated that by using Rpl32 as the loading control.

Samples of the monosomes and polysomes were run on 16% Tris–Glycine Mini Protein Gels (Lifetechnologies catalog number: EC6498BOX) for 100 min using the instructions of the manufacturer. The proteins were blotted using the semi-dry method and CAPS buffer at pH 11 on PVDF membrane. The RPs were detected with antibodies from Santa Cruz Biotechnology, Inc, Catalog Numbers: sc-25931 for Rpl11, sc-133977 for Rpl32, sc-68873 for Rps14, and sc-133962 for Rps29. After incubation with secondary antibodies and visualization with Super-Signal West Femto Chemiluminescent Substrate (Thermo Scientific, catalog number 34095), all antibodies resulted in a single band at the molecular weight corresponding to the cognate RP. The blots were imaged with AlphaImager System, and the images were quantified with Image Studio Lite, version 4.0. Consistent with the MS data (Figure S3A), the Western Blots data (Figure S3B) indicate that Rps29 and Rps14 are enriched in polysomes, Rpl11 is enriched in monosomes, and Rpl32 does not change (loading control).

Correlation between relative RP levels and fitness

To explore the physiological significance (if any) of the altered RP stoichiometry, we computed the correlation between the fitness of yeast strains with single RP-gene deletions (Qian *et al*, 2012) and the corresponding relative RP levels that we measured (Figure 3). In yeast, 21 pairs of RP-genes encode proteins with identical amino acid sequences within a pair. Since the RPs within these 21 pairs cannot be distinguished by MS, these 21 RPs were excluded from our analysis and not used to compute correlations between RP levels and fitness of RP-delete strains. Furthermore, some RPs that we quantified did not have RP-deletion fitness data and thus could not be included in our correlation analysis.

Supplementary Discussion

Evaluation of factors that may affect the measured RP levels

The estimated RP levels (Figures 1-3) appear to vary significantly between monosomes and polysomes and across the growth conditions. However, this variation might reflect not only stoichiometry changes among the RPs but also other factors and artifacts, such as noise in the MS measurements, a differential distribution of nascent RP polypeptides among monosomes and polysomes, posttranslational modifications (PTMs) of the RPs, and the presence of 90S ribosomal biogenesis particles. In the subsections below we describe our investigation of such potential artifacts. The results of this investigation (Figure S2 and Figure S4), indicate that such potential artifacts are unlikely to contribute significantly to the estimated RP levels (Figures 1-3), suggesting that the stoichiometry among the RPs can change across polyribosomes and physiological conditions in the absence of genetic perturbations.

Noise, coisolation interference and posttranslational modifications (PTMs)

From most RPs, we quantify multiple unique peptides (whose amino acid sequence is found only in one RP and no other protein in the proteome) both in mouse (Figure S2A, C) and in yeast (Figure S2E). In the absence of measurement noise, post-translational modifications (PTMs), or partial peptides (such as nascent poly-peptide chains), the fold-changes of an RP should equal the fold-changes of each unique peptide coming from this RP. Thus the similarity between the fold changes of unique peptides for the same RP, as quantified by the coefficient of variation (CV; the ratio of the standard deviation to the mean), reflects the degree to which the estimated fold–changes for an RP are influenced by post-translational modification, by noise, and by partial protein products. To evaluate the contribution of all these factors to our RP quantification (Figures 1-3), we computed the distributions of CV values for mouse (Figure S2B, D) and for yeast (Figure S2F) for all RPs having multiple quantified unique peptides per RP. These distributions indicate a median CV < 0.25 and thus suggest that PTMs, measurement noise and partial RPs are not dominant factors in the quantification of most RPs. A few fold-changes, however, have larger CVs that might reflect either PTMs or larger noise in the peptide quantification.

Coisolation interference in the quantification of the reporter ions results in underestimation of the fold changes (Bantscheff *et al*, 2007). To reduce the influence of coisolation interference, we filtered out the quantified peptides with large coisolation interference.

Differential distribution of nascent RP polypeptides among monosomes and polysomes

In principle, a differential distribution of nascent RP polypeptides among monosomes and polysomes could contribute to the measured RP changes (Figures 1-3). As discussed above, the low CVs for protein fold-changes quantified from different unique peptides (Figure S2) make this possibility unlikely.

We sought to test the possibility that nascent RP polypeptides contribute to our estimates of RP levels even more directly. First, if nascent RPs contribute significant numbers of peptides to the variation in RP levels in Figures 1-3, the MS1 precursor-area (integrated area under the MS1 spectrum of the precursor ions that reflects peptide abundance) of N-terminal peptides would be higher compared to the MS1 precursor-area of C-terminal peptides. We compared the distributions of MS1 precursor-areas for N-terminal peptides and for C-terminal peptides and found that the two distributions are statistically identical both for yeast and for mouse. This result suggests that nascent RPs do not contribute significantly to the measured changes in the RP stoichiometry. Second, our Western blots for Rpl11, Rps29, Rps14, and Rps32 showed only one band at the expected molecular weight and no lower molecular weight bands that would correspond to growing nascent chains. If present at a significant level in the sucrose fractions, such growing nascent chains should be detected by the antibodies recognizing N-terminal epitops. Indeed, even in the most extreme case when all mRNAs translated by the ribosomes code for RPs, peptides contributed by the nascent chains are less than $1/80 = 1.2\ \%$ of all RP peptides from a digested fraction. Third, some very short RPs, such as Rps29, which is only 56 animo acids long (6.6 kDa), are highly enriched in the mouse fractions having 7-10 ribosomes per mRNA. The mRNA coding for Rps29 cannot physically fit 7-10 ribosomes, and thus the polysomal enrichment of Rps29 and other short RPs cannot possibly be explained by the on-going translation of nascent poly-peptides in the mouse polysomes. More generally, if nascent proteins contribute to the measured variability, our estimates should indicate that longer

RPs are enriched in sucrose fractions having more ribosomes per mRNA since longer mRNA are translated by more ribosomes (Arava *et al*, 2003). We find no such enrichment, suggesting that our measurements are not significantly affected by nascent polypeptide chains. This is particularly clear in the mouse dataset where we quantified sucrose fractions corresponding to 7-10 ribosomes per mRNA.

The 90S ribosomal biogenesis particles

Sucrose gradients separate not only mature ribosomes but also other cellular organelles of comparable size, such as the immature 90S ribosomal biogenesis particles (Granneman and Baserga, 2004; Sykes and Williamson, 2009; Sykes *et al*, 2010; Chen and Williamson, 2013). The 90S particles should have unequal distribution across the gradient, localizing closely to the 80S monosomal peak and decreasing toward the higher sedimentation-velocity region of the polysomes. Thus if the amount of 90S particles is comparable to the amount of ribosomes, 90S particles could contribute significantly to the changes in the RP stoichiometry in Figures 1-3. However, in exponentially growing cells, the 90S ribosomal biogenesis particles are less abundant than the mature ribosomes (Granneman and Baserga, 2004; Sykes and Williamson, 2009; Sykes *et al*, 2010; Chen and Williamson, 2013), and thus unlikely to contribute substantially to the RP peptides that we quantified.

We used our data to evaluate the extent to which immature 90S particles contribute to our estimates of variability among the RPs. Two key factors that determine this contribution are (i) the level and (ii) the sucrose-gradient localization of the 90S. To estimate these two factors, we used the ribosome-biogenesis proteins that are known to be associated with the 90S particle but not with the mature ribosomes (Granneman and Baserga, 2004). These ribosome-biogenesis proteins provide a solid basis for estimating the abundance of the 90S particles relative to the mature ribosomes and the distribution of the 90S particles across the sucrose fractions.

First, we estimated the abundance of the 90S particle relative to the mature ribosomes. From the 180 proteins annotated by the gene ontology (GO:0042254) term "ribosome biogenesis," we have quantified unique peptides for only 14 proteins that are not core structural RPs. These 14 ribosome-biogenesis proteins are represented in our data by very few peptides (9 proteins are represented by a single peptide), which likely reflects the low abundance of these proteins (relative to the RPs) in our sucrose fractions. This conclusion is strongly supported by the

low MS1 precursor-area (integrated area under the MS1 spectrum of the precursor ions) of ribosome-biogenesis peptides compared to the MS1 precursor-area of RP peptides. To obtain a more quantitative estimate for the abundance of 90S relative to the mature ribosomes, we computed and compared the iBAQ scores (Schwanhäusser *et al*, 2011) (a popular measure for absolute protein levels) for the RPs and for the ribosome biogenesis proteins. The iBAQ scores indicate that the detected ribosome biogenesis proteins and thus the 90S particles are about 100 times less abundant than the RPs and thus the mature ribosomes (Figure S4A), consistent with previous observations (Sykes *et al*, 2010).

The mass-spectrometry method used in our study estimates the absolute levels of a peptide from MS1-level integrated-precursor-ion-area, while the relative levels of a peptide/protein across the samples are estimated from MS2-level reporter-ion-intensities. At the MS1-level, the peptides having the same amino-acid sequence from all samples/fractions are quantified as one integrated-precursor-ion-area, and their relative levels across the samples can be estimated only after fragmentation of the precursor ions, i.e., at the MS2 level. Thus the MS1 data that allow direct absolute quantification – and thus comparing the abundances of different proteins – quantifies the total/cumulative amount for each protein in all analyzed fractions. These data were used to estimate iBAQ scores that reflect the absolute levels for both RPs and ribosome biogenesis factors (Figure S4A). We further used the reporter-ion-intensities to quantify the relative levels of all identified proteins. This relative quantification shows that, as expected, ribosome biogenesis factors are enriched in the monosomal fractions. Combining the absolute and the relative quantification, we estimated the absolute levels of RPs and biogenesis factors only in the monosomal fractions (Figure S4B); specifically, the absolute level of a protein in the monosomal fractions equals its iBAQ score times the sum of its reporter-ion-intensities from the monosomal fractions and divided by the sum of its reporter-ion-intensities in the all fractions. These estimates show that even in the monosomal fractions, biogenesis factors are much less abundant than RPs (Figure S4B), and thus ribosome-biogenesis complexes are likely much less abundant than mature ribosomes. The low abundance of ribosome-biogenesis complexes makes them unlikely to contribute significantly to the quantified RP levels. More quantitatively, the data suggest that the proteins derived from the 90S can contribute about $1-3\ \%$ to the RP fold-changes. Since some measured RP fold-changes exceed $100\ \%$, 90S particles are unlikely to be the sole factor causing the differential RP stoichiometry that we measured.

Second, as expected, the 90S ribosome biogenesis peptides are localized to the 80S monosomal fraction and their levels are even lower and constant across the rest of the sucrose gradient. Thus their small contribution is limited to the monosomes and cannot account for the relative RP changes across polysomes that we observed both in yeast and in mouse (Figures 1-3).

Extra-ribosomal complexes of RPs

A few RPs have been reported to perform extra-ribosomal functions (Mazumder *et al*, 2003; Wool, 1996; Warner and McIntosh, 2009). Some of these extra-ribosomal functions of RPs are performed by small complexes containing RPs. For example a Rpl5/Rpl11/5S-rRNA preribosomal complex is involved in the regulation of p53 (Donati *et al*, 2013). Such extra-ribosomal complexes containing RPs are smaller than the mature ribosomes and should not co-sediment in the sucrose fractions that we analyzed (Donati *et al*, 2013; Warner and McIntosh, 2009). This expectation is strongly supported by our MS data: the non ribosomal proteins identified by our MS analysis included translation factors and protein-folding chaperones, but not proteins known to be involved in extra-ribosomal complexes of RPs. Thus, the levels of extra-ribosomal complexes of RPs that may be present in the analyzed sucrose fractions were too low to be detected by and to affect our analysis.

Stoichiometry among RPs

Our data show that while the levels of some RPs increase, the levels of other RPs decrease. These opposite trends indicate that the ratios (stoichiometries) among RPs making up monosomes and polysomes vary. However, our population–average measurements do not indicate the number of distinct ribosomes in each sucrose fraction or the exact RP composition of such distinct ribosomes.

RPs of the small (40S) and the large (60S) subunits are about equally represented among the subset of RPs that increase or decrease across monosomes and polysomes, Figures 1-3. Therefore, preferential enrichment of 40S or 60S in some fractions is very unlikely to contribute to the variation among RPs that we observe.

References

Aebersold R, Burlingame AL, Bradshaw RA (2013) Western blots versus selected reaction monitoring assays: time to turn the tables? *Molecular Cellular Proteomics* **12**: 2381–2382

Altelaar A, Frese CK, Preisinger C, Hennrich ML, Schram AW, Timmers H, Heck AJ, Mohammed S (2013) Benchmarking stable isotope labeling based quantitative proteomics. *Journal of proteomics* **88**: 14–26

Arava Y, Wang Y, Storey JD, Liu CL, Brown PO, Herschlag D (2003) Genome-wide analysis of mRNA translation profiles in *Saccharomyces cerevisiae*. *Proceedings of the National Academy of Sciences* **100**: 3889–3894

Bantscheff M, Schirle M, Sweetman G, Rick J, Kuster B (2007) Quantitative mass spectrometry in proteomics: a critical review. *Analytical and bioanalytical chemistry* **389**: 1017–1031

Blagoev B, Ong SE, Kratchmarova I, Mann M (2004) Temporal analysis of phosphotyrosine-dependent signaling networks by quantitative proteomics. *Nature biotechnology* **22**: 1139–1145

Brauer MJ, Huttenhower C, Airoldi EM, Rosenstein R, Matese JC, Gresham D, Boer VM, Troyanskaya OG, Botstein D (2008) Coordination of Growth Rate, Cell Cycle, Stress Response, and Metabolic Activity in Yeast. *Mol Biol Cell* **19**: 352–367

Chen SS, Williamson JR (2013) Characterization of the Ribosome Biogenesis Landscape in *E. coli* Using Quantitative Mass Spectrometry. *Journal of molecular biology* **425**: 767–779

Cottrell J, London U (1999) Probability-based protein identification by searching sequence databases using mass spectrometry data. *Electrophoresis* **20**: 3551–3567

Cox J, Mann M (2008) MaxQuant enables high peptide identification rates, individualized ppb-range mass accuracies and proteome-wide protein quantification. *Nature biotechnology* **26**: 1367–1372

Donati G, Peddigari S, Mercer CA, Thomas G (2013) 5S ribosomal RNA is an essential component of a nascent ribosomal precursor complex that regulates the Hdm2-p53 checkpoint. *Cell reports* **4**: 87–98

Eng JK, McCormack AL, Yates Iii JR (1994) An approach to correlate tandem mass spectral data of peptides with amino acid sequences in a protein database. *Journal of the American Society for Mass Spectrometry* **5**: 976–989

Granneman S, Baserga SJ (2004) Ribosome biogenesis: of knobs and RNA processing. *Experimental cell research* **296**: 43–50

Hickman M, Winston F (2007) Heme levels switch the function of Hap1 of *Saccharomyces cerevisiae* between transcriptional activator and transcriptional repressor. *Molecular and Cellular Biology* **27**: 7414–7424

Jenner L, Melnikov S, de Loubresse NG, Ben-Shem A, Iskakova M, Urzhumtsev A, Meskauskas A, Dinman J, Yusupova G, Yusupov M (2012) Crystal structure of the 80S yeast ribosome. *Current opinion in structural biology* **22**: 759–767

Lu P, Vogel C, Wang R, Yao X, Marcotte EM (2006) Absolute protein expression profiling estimates the relative contributions of transcriptional and translational regulation. *Nature biotechnology* **25**: 117–124

Mazumder B, Sampath P, Seshadri V, Maitra RK, DiCorleto PE, Fox PL (2003) Regulated release of L13a from the 60S ribosomal subunit as a mechanism of transcript-specific translational control. *Cell* **115**: 187–198

Mulder AM, Yoshioka C, Beck AH, Bunner AE, Milligan RA, Potter CS, Carragher B, Williamson JR (2010) Visualizing ribosome biogenesis: parallel assembly pathways for the 30S subunit. *Science* **330**: 673–677

Ong SE, Blagoev B, Kratchmarova I, Kristensen DB, Steen H, Pandey A, Mann M (2002) Stable isotope labeling by amino acids in cell culture, SILAC, as a simple and accurate approach to expression proteomics. *Molecular cellular proteomics* **1**: 376–386

Peng M, Taouatas N, Cappadona S, van Breukelen B, Mohammed S, Scholten A, Heck AJ (2012) Protease bias in absolute protein quantitation. *Nature methods* **9**: 524–525

Qian W, Ma D, Xiao C, Wang Z, Zhang J (2012) The genomic landscape and evolutionary resolution of antagonistic pleiotropy in yeast. *Cell Reports* **2**: 1399–1410

Schwanhäusser B, Busse D, Li N, Dittmar G, Schuchhardt J, Wolf J, Chen W, Selbach M (2011) Global quantification of mammalian gene expression control. *Nature* **473**: 337–342

Slavov N, Botstein D (2011) Coupling among growth rate response, metabolic cycle, and cell division cycle in yeast. *Molecular Biology of the Cell* **22**: 1997–2009

Slavov N, Budnik B, Schwab D, Airoldi E, van Oudenaarden A (2014) Constant Growth Rate Can Be Supported by Decreasing Energy Flux and Increasing Aerobic Glycolysis. *Cell Reports* **7**: 705 – 714

Slavov N, Macinskas J, Caudy A, Botstein D (2011) Metabolic cycling without cell division cycling in respiring yeast. *Proceedings of the National Academy of Sciences of the United States of America* **108**: 19090–19095

Sykes MT, Shajani Z, Sperling E, Beck AH, Williamson JR (2010) Quantitative Proteomic Analysis of Ribosome Assembly and Turnover *In Vivo*. *Journal of molecular biology* **403**: 331–345

Sykes MT, Williamson JR (2009) A complex assembly landscape for the 30S ribosomal subunit. *Annual review of biophysics* **38**: 197–215

Warner JR, McIntosh KB (2009) How common are extraribosomal functions of ribosomal proteins? *Molecular cell* **34**: 3–11

Wiśniewski J, Zougman A, Nagaraj N, Mann M (2009) Universal sample preparation method for proteome analysis. *Nature methods* **6**: 359–362

Wool IG (1996) Extraribosomal functions of ribosomal proteins. *Trends in biochemical sciences* **21**: 164–165

Supplemental Figures

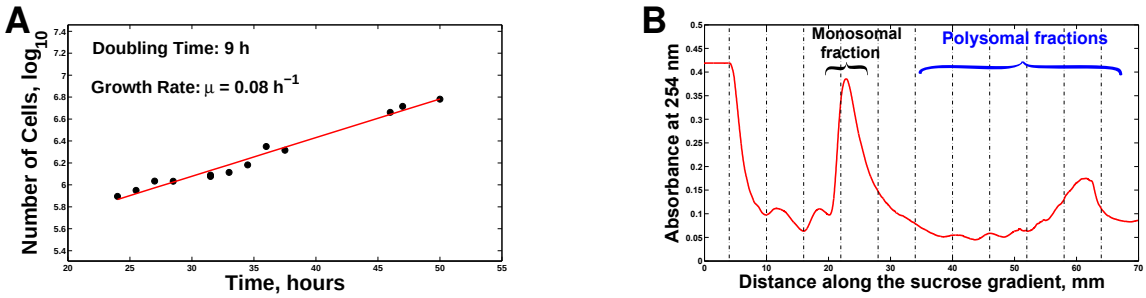

Figure S1. Growth curve of mouse ESCs and a sucrose gradient of neuroprogenitor cells, Related to Figure 1

(**A**) Growth curve of mouse ESCs. At time 0h, 15 ESC cultures were started, and at each time point indicated on the x-xis, one culture was harvested to determine the cell number (y-axis). The cell number is plotted on a log-scale. The data indicate rapid exponential growth at a doubling time of about 9 hours. The ESCs used for our analysis were harvested during the middle of the curve, 35 h after starting the cultures.

(**B**) Sucrose gradient of neuroprogenitor cells (NPCs). The ESCs used in our experiments were differentiated to NPCs, and the ribosomes of the NPCs were fractionated by velocity sedimentation using identical protocol and treatment as those used with ESCs; see the Methods and Extended Appendix for detailed description of the velocity sedimentation.

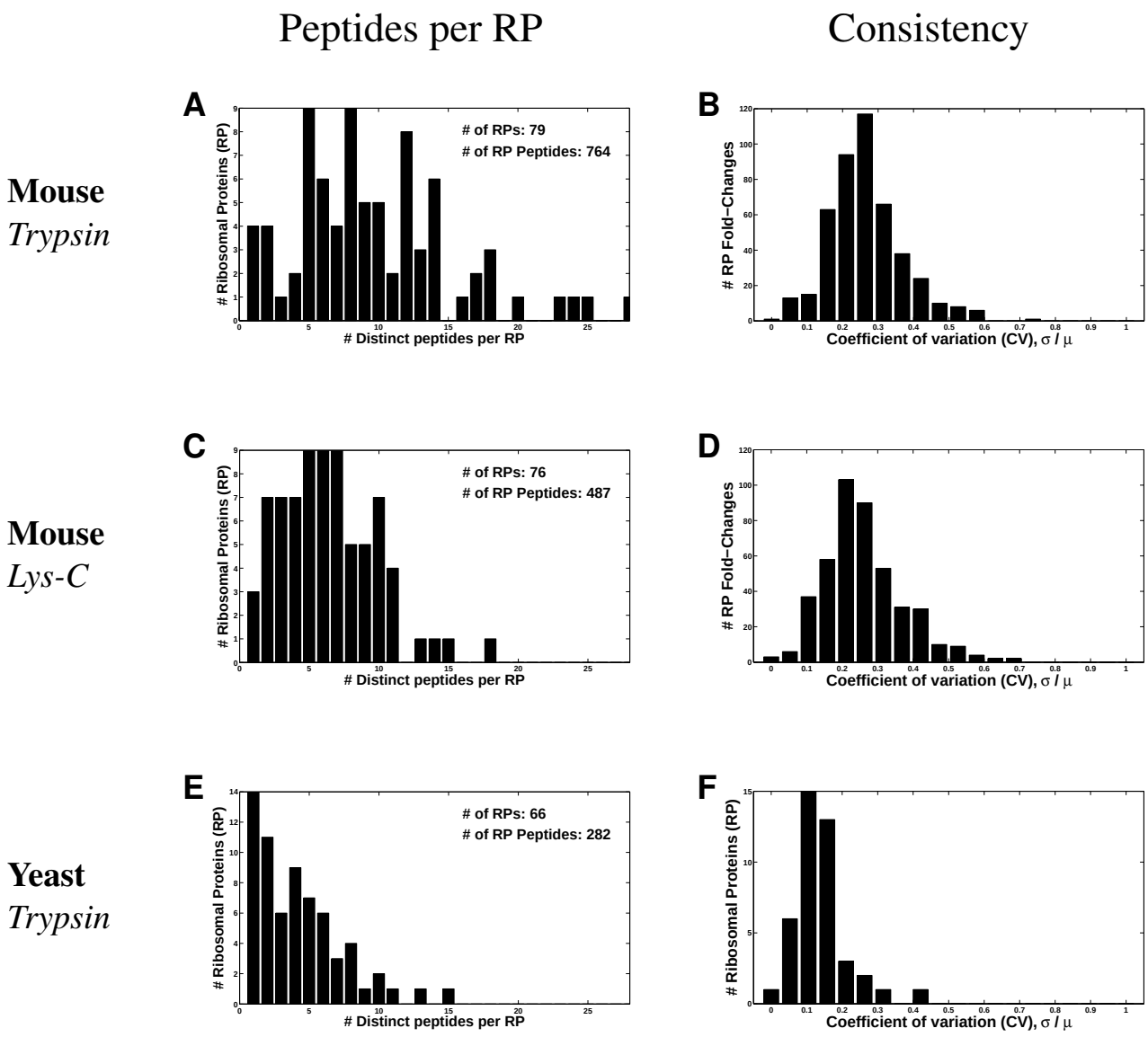

Figure S2. Multiple unique peptides per RP provide consistent fold–change estimates for most RPs, Related to Figures 1-3

(**A**) Number of unique peptides quantified per mouse RP digested by trypsin.

(**B**) Distribution of coefficients of variation (CVs) of the measured fold–changes for mouse RPs digested by trypsin.

(**C**) Number of unique peptides quantified per mouse RP digested by lys-C.

(**D**) Distribution of coefficients of variation (CVs) of the measured fold–changes for mouse RPs digested by lys-C.

(**E**) Number of unique peptides quantified per yeast RP digested by trypsin.

(**F**) Distribution of coefficients of variation (CVs) of the measured fold–changes for yeast RPs digested by trypsin.

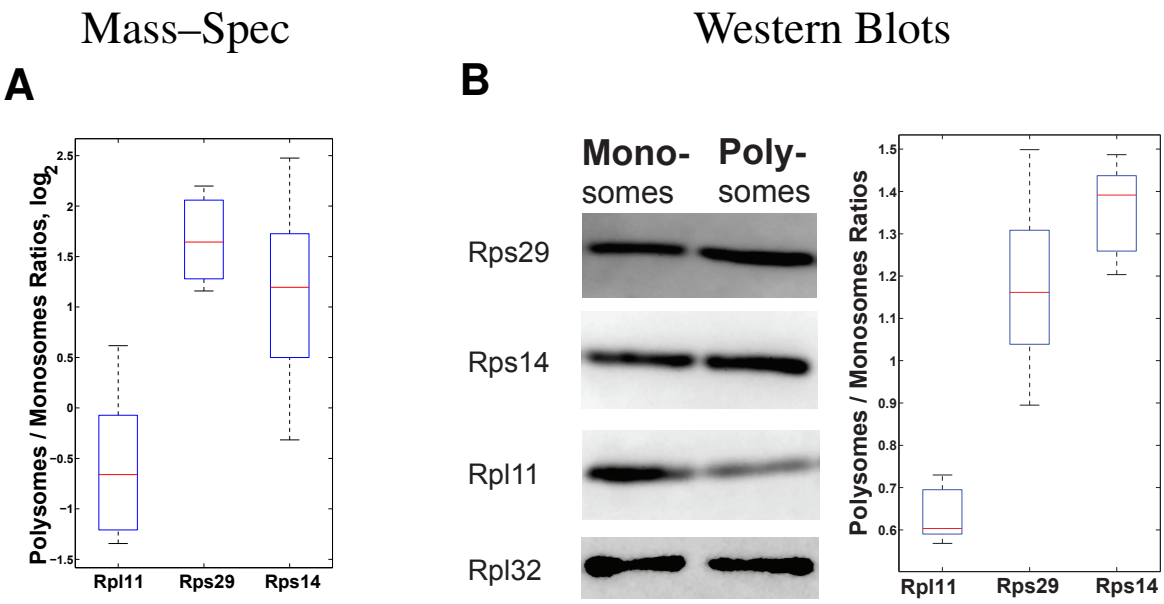

Figure S3. Comparison of relative RP quantification by MS and Western Blots, Related to Figures 1-2.

(**A**) Polysomal enrichment of RPs quantified by MS.

(**B**) Polysomal enrichment of RPs quantified by Western blots. RPs were quantified by Western blots in monosomes and polysomes from high passage–number E14 mouse ESCs. Rpl32 was used as a loading control and the boxplots summarize data from 9 ratios for each quantified RP.

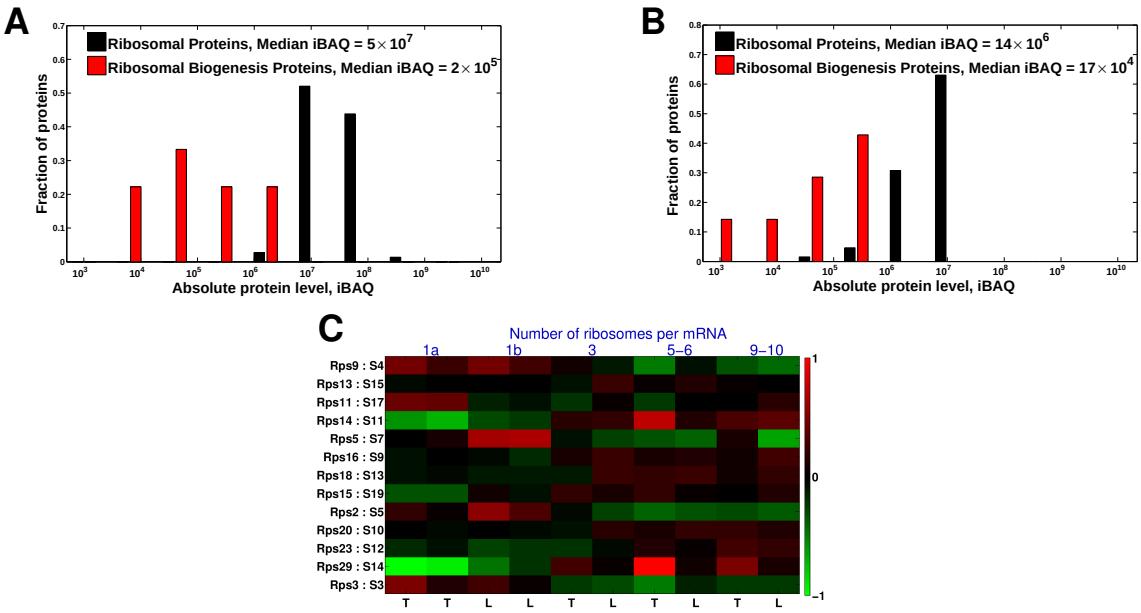

Figure S4. RPs are about 100 fold more abundant that ribosome biogenesis proteins in the sucrose gradients, Related to Figures 1-3

(**A**) Distributions of iBAQ scores for RPs and for ribosome biogenesis proteins. The iBAQ score of a protein estimates its absolute level based on the number of unique peptides for that proteins and their corresponding integrated-precursor-ion-areas. The iBAQ scores are for the total/cumulative amount in all analyzed fractions. The levels of ribosome biogenesis proteins likely reflect the levels of the 90S preribosomal particles in our sucrose gradients.

(**B**) The data from panel (A) was scaled by the reporter-ion intensities to estimate the abundances of RPs and ribosome biogenesis proteins in the monosomal fractions only.

(**C**) The relative levels of mouse RPs are plotted as in Figure 2 but the RPs are arranged in the order in which they are incorporated into the small subunits, as determined by Mulder *et al* (2010); RPs at the top are incorporated first and RPs as the bottom last. Mouse and bacterial RPs were matched based on the correspondence suggested by Jenner *et al* (2012), and the suggested universal ID is listed after the colon.

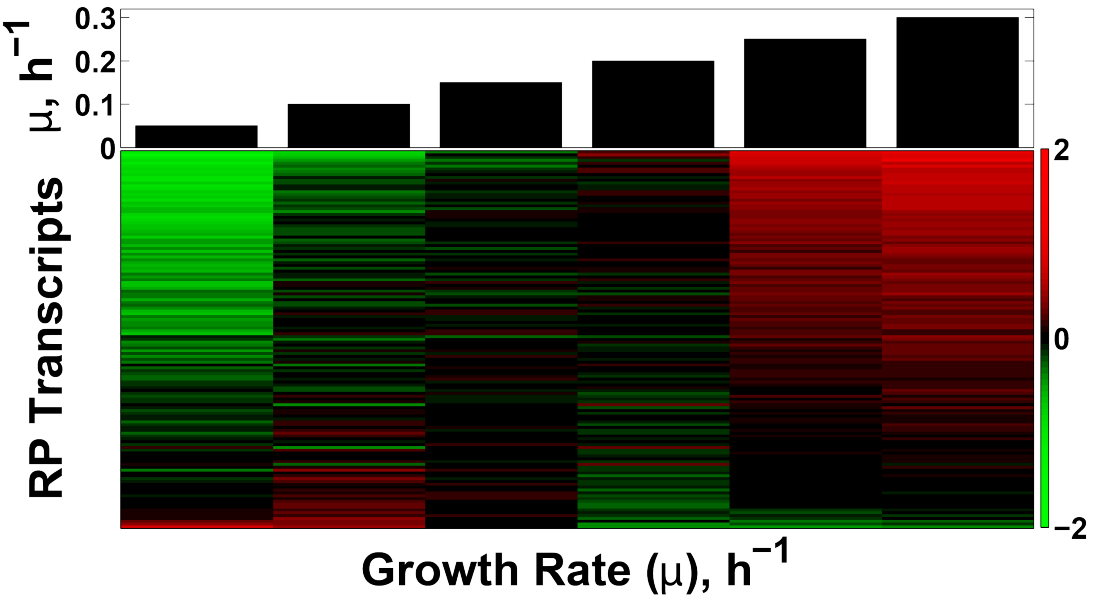

Figure S5. Different RPs have different magnitudes of their growth-rate responses, i.e., transcriptional induction or repression with increasing growth rate, Related to Figure 4. The heatmap displays transcript levels of RPs in yeast cultures growing at steady-state in glucose-limited minimal media at the growth-rates (μ) indicated by the bars on the top. To emphasize the growth-rate trends, the mRNA levels of each RP are displayed on a log_2 scale relative to their mean across all six growth rates. The RPs are sorted by their growth-rate slopes to emphasize the variability of their slopes, from highly positive to negative. All data are from (Slavov and Botstein, 2011; Brauer *et al*, 2008).

Supplemental Tables

Table S1. Normalized protein levels (on a log_2 scale) that are displayed in Figure 2
To facilitate comparison between orthologous RPs, we include the names from the nomenclature suggested by Jenner *et al* (2012).

Table S2. MS data for mouse peptides from the trypsin digestion, Figure 1 and Figure 2
The map of the reporter ions and their corresponding samples from the sucrose gradients is as follows:
TMT-126 – Sucrose fraction corresponding to 1 ribosome per mRNA;
TMT-127 – Sucrose fraction corresponding to 3 ribosome per mRNA;
TMT-129 – Sucrose fraction corresponding to 5-6 ribosome per mRNA;
TMT-130 – Sucrose fraction corresponding to 7-10 ribosome per mRNA;
TMT-131 – Sucrose fraction corresponding to 1 ribosome per mRNA;

Table S3. MS data for mouse peptides from the lys-C digestion, Figure 1 and Figure 2
The map of the reporter ions and their corresponding samples from the sucrose gradients is as follows:
TMT-126 – Sucrose fraction corresponding to 1 ribosome per mRNA;
TMT-127 – Sucrose fraction corresponding to 3 ribosome per mRNA;
TMT-129 – Sucrose fraction corresponding to 5-6 ribosome per mRNA;
TMT-130 – Sucrose fraction corresponding to 7-10 ribosome per mRNA;
TMT-131 – Sucrose fraction corresponding to 1 ribosome per mRNA;

Table S4. Normalized protein levels (on a log_2 scale) that are displayed in Figure 3
To facilitate comparison between orthologous RPs, we include the names from the nomenclature suggested by Jenner *et al* (2012).

Table S5. MS data for yeast peptides from the lys-C digestion, Figure 3
The map of the reporter ions and their corresponding samples from the sucrose gradients is as follows:
TMT-131 – Ethanol: Sucrose fraction corresponding to 1 ribosome per mRNA; Biological replicate 1a
TMT-128N – Ethanol: Sucrose fraction corresponding to 1 ribosome per mRNA; Biological replicate 1b
TMT-128C – Ethanol: Sucrose fraction corresponding to 3 ribosome per mRNA;
TMT-129N – Ethanol: Sucrose fraction corresponding to 4 ribosome per mRNA;
TMT-129C – Glucose: Sucrose fraction corresponding to 1 ribosome per mRNA;
TMT-130N – Glucose: Sucrose fraction corresponding to 3 ribosome per mRNA;
TMT-130C – Glucose: Sucrose fraction corresponding to 4 ribosome per mRNA;